

On the Mass Transport and the Crystal Growth in a Freeze Lining of an Industrial Nonferrous Slag

MIEKE CAMPFORTS, KAREL VERSCHEURE, EDDY BOYDENS, TIM VAN ROMPAEY, BART BLANPAIN, and PATRICK WOLLANTS

Lab scale freeze layers of an industrial nonferrous slag with as main components Al_2O_3 - CaO - FeO_x - MgO - SiO_2 - ZnO were studied to explore the mass transport in an industrial freeze lining. The freeze layers were formed by submerging a water-cooled probe into a liquid slag bath. In previous research,^[1] two distinct types of microstructures were observed in these freeze layers: one with only melilite columnar crystals and one with both melilite and olivine columnar crystals. In this article, the mass transport during the formation of these microstructures is investigated. The element distribution, the phase fraction, and the crystal morphology were examined using electron microscopy and electron probe microanalysis. In addition, thermodynamic software was used to calculate the solidification path of the slag. The impact of the mass transport on the growth of a freeze lining depends on the solidification rate. For high solidification rates, only short-range mass transport is observed and small crystals form. For lower solidification rates, long-range mass transport is observed, resulting in an exchange of components between the freeze layer and liquid slag bath and in the formation of large crystals. Different growth mechanisms are observed for melilite and olivine crystals. The broad large melilite crystals have to exchange components with the liquid slag bath to grow, because the amount of liquid slag between the crystals is limited, while the long thin olivine crystals can exchange components with a large amount of liquid slag in between the crystals. Furthermore, the mass transport of minor elements may be very important, because these elements can pile up at the crystal-liquid slag interface and hamper the crystal growth.

DOI: 10.1007/s11663-008-9141-y

© The Minerals, Metals & Materials Society and ASM International 2008

I. INTRODUCTION

SEVERAL pyrometallurgical processes operate with high intensity conditions, such as high process temperature, strong convection in the bath, and aggressive process materials. Examples are slag cleaning,^[2,3] zinc fuming,^[4,5] ilmenite smelting,^[6-8] and the Hall-Héroult process.^[9-12] These processes pose challenges related to reactor integrity and the life of the refractory reactor wall. To extend the life of the refractory wall, the wall is often cooled. As a result, a solid crust of process material, also referred to as a freeze lining, a freeze layer, or a side ledge, may form on the hot side of the refractory wall. In some processes, such as ilmenite smelting and the Hall-Héroult process, a freeze lining is the best solution to reach an acceptable campaign time.^[6-9]

A freeze lining is the result of a thermal balance between heat input from the liquid bath and heat

removal by the cooling medium, as illustrated in Figure 1. In steady state, the heat input equals the heat removal and the freeze lining thickness remains constant. Any imbalance between heat input and heat removal results in growth or melting of the freeze lining to re-establish steady state at another thickness. Furthermore, industrial process materials are often multi-component systems. Therefore, the freeze lining composition may not equal that of the bath material. In this case, components are exchanged between the freeze lining and the bath when the freeze lining grows or melts. Thus, the growth of the freeze lining can be a complex combination of mass transport and heat transport.

Because the process materials in the high-intensity processes are highly corrosive for the refractory wall, the formation of a freeze layer has to be guaranteed. Process material has to form a layer of solids on the reactor wall. Furthermore, this layer has to remain attached to the refractory wall and ideally does not spall. If the layer does spall, a new layer should form immediately. A better understanding of freeze lining behavior is thus necessary to establish process conditions for an optimal protection of the refractory wall. The microstructure of a freeze lining is very useful here, because it contains information on the freeze layer formation and on the hot face temperature, and it determines the physical, mechanical, and chemical properties of the freeze lining.

MIEKE CAMPFORTS, Research Assistant, and BART BLANPAIN and PATRICK WOLLANTS, Full Professors, are with the Centre for High Temperature Processes, Metallurgy and Refractory Materials, Department of Metallurgy and Materials Engineering, Katholieke Universiteit Leuven, B-3001 Leuven, Belgium. Contact e-mail: Mieke.Campforts@mtm.kuleuven.be KAREL VERSCHEURE and TIM VAN ROMPAEY, Project Leaders, and EDDY BOYDENS, Manager Analytical Laboratory, are with Umicore Research, B-2250 Olen, Belgium.

Manuscript submitted September 25, 2007.

Article published online June 6, 2008.

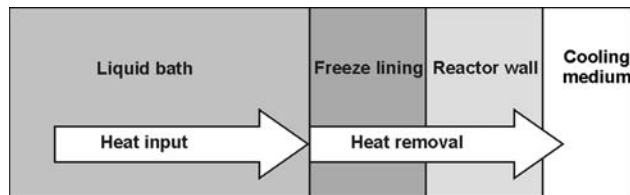


Fig. 1—Schematic representation of the heat transport in a freeze lining.

The microstructure of a freeze lining has been studied for cryolite salts of the Hall–Héroult process^[9,10] and for some industrial nonferrous slags.^[1,13] In the Hall–Héroult cell, at high solidification rates, an amorphous freeze layer forms with a composition close to the bath, while at intermediate cooling rates, dendrites of primary phase form, entrapping bath material between the dendrites.^[9,10] The composition of the freeze layer will vary from the primary phase according to the phase diagram at low solidification rates to the bath composition at high rates. Clearly, the solidification rate influences the mass transport of components between the freeze layer and bath. The freeze lining microstructure of the industrial nonferrous slags is also dependent on the solidification rate.^[1,13] At high cooling rates, an amorphous phase forms. At intermediate cooling rates, columnar crystals form, which do not consist of the primary phase but of melilite (the secondary phase) or, in some microstructures, even of olivine (the last phase to form during equilibrium solidification). These two microstructure types are observed for similar experimental conditions and even within the same lab scale freeze layer.^[1] The formation and the selection of the two microstructure types are not well understood. Unlike the cryolite freeze lining, the composition of the slag freeze linings more or less equals the bath composition for high to intermediate cooling rates. The research on the microstructure of slag freeze lining is still explorative. Important questions are how the mass transport occurs and how it affects crystal growth during the formation of a freeze layer.

The goal of the research is to explore the mass transport in an industrial freeze lining of a nonferrous slag. In this article, the element distribution, the phase fractions, and the crystal morphology in the freeze layers are investigated to understand the mass transport during freeze lining formation and its influence on crystal growth for the two microstructure types observed in previous research. These types are further referred to as A (melilite columnar crystals) and B (melilite and olivine columnar crystals).

II. EXPERIMENTAL

A. Water-Cooled Probe Technique

The experimental setup (also References 1 and 13) is shown in Figure 2. A 30-kW open induction furnace heats a SiC crucible containing a second crucible with the slag. Bath temperatures up to 1500 °C are achievable.

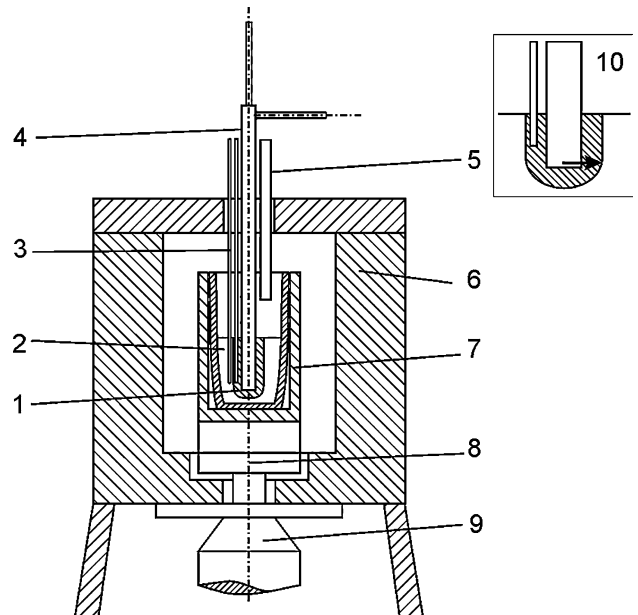


Fig. 2—Schematic drawing of the experimental setup: (1) freeze layer; (2) liquid slag bath; (3) thermocouples fixed to the probe at a constant distance from the probe's surface; (4) water-cooled probe; (5) protective gas blowing tube; (6) induction furnace; (7) crucible; (8) rotational disk; (9) motor; and (10) detail of the freeze layer, the arrow indicates the sampling location for SEM and EPMA.



Fig. 3—Schematic drawing of the water-cooled probe. The arrows indicate the direction of the water flow.

The crucibles are placed on a rotational disk with variable speed from 0 to 28.5 rpm. A water-cooled probe is submerged into the molten slag to form a freeze layer. The probe is made of stainless steel and its design is shown in Figure 3. The cooling water enters the probe through the inner tube (7.5 mm diameter) and leaves it through the outer tube (15 mm diameter, 600 mm length). Two thermocouples are attached at 1 and 2 cm from the probe's surface (Figure 2, item 3). A removable thermocouple is used to measure the slag bath temperature before and after submerging the probe.

The experimental procedure is as follows: a SiC crucible containing an Al₂O₃ crucible with 3 kg of crushed slag (4 to 28 mm) is heated in the inductive furnace, while N₂ is blown over the slag (100 L/h). When the targeted bath temperature (1365 °C to 1375 °C) is reached, a sample of the “start slag” bath is taken with a cold steel rod and quenched in liquid nitrogen in order to prevent oxidation. Next, the thermocouple for measuring the slag bath temperature is removed and the water-cooled probe with the two

fixed thermocouples is submerged 9 cm into the bath for 30 minutes to form a freeze layer. During submergence, the rotational speed of the crucible (5.7 rpm), the water flow rate (4 to 5 L/h), and the furnace power (20 kW) are kept constant. At the end of the experiment, the probe with the freeze layer is removed from the slag bath and cooled in a nitrogen atmosphere. After replacing the slag bath thermocouple and reheating the slag to the starting temperature, an “end slag” bath sample is taken using the same procedure as for the “start slag” bath sample. The samples studied in this article are taken from two different experiments, A and B, with corresponding microstructure types A and B.

B. Analysis

The composition of the slag bath samples is determined by fusing the sample with Na_2O_2 and leaching with HCl. The resulting liquid is analyzed using inductively coupled plasma–atomic emission spectroscopy. The Fe^{2+} amount is determined by partly dissolving the sample in a HF and H_2SO_4 solution. O-phenantroline is added to the solution to form a complex. The whole is analyzed with UV-VIS spectrometry. The Fe^{3+} amount is the difference between the total Fe amount and the Fe^{2+} amount. Only the samples of experiment A are analyzed for Fe^{2+} .

For scanning electron microscopy (SEM) and electron probe microanalysis (EPMA), a sample is taken at the bottom part of the freeze layer (Figure 2(10)). The SEM is used in backscattered electron mode at a 10-kV acceleration voltage. The EPMA using wavelength dispersive spectroscopy is performed with a reference current of 30 nA in the willemite standard at 20-kV acceleration voltage.

C. Industrial Nonferrous Slag

The composition of the industrial nonferrous slag, as received from the lead blast furnace process, is shown in Table I. Iron is present as Fe^{2+} and Fe^{3+} . The slag also contains small amounts of minor elements, such as Pb, S, Ba, Cr, Sr, Cu, Sn, Mn, and K that are not accounted for in Table I. Their concentrations vary between 0.3 and 1 wt%. Table I also shows the ratio of network breaking cations (NBC: Ca^{2+} , Fe^{2+} , Fe^{3+} , Zn^{2+} , and Mg^{2+} ; here, Fe^{3+} is considered to be a NBC because its fraction in the slag is very limited) to network forming cations (NFC: Al^{3+} and Si^{4+}).

Tables II and III show the composition and the NBC/NFC ratio of the start and end slag bath for A and B, respectively. The deviation from the slag as received is within experimental error. The $\text{Fe}^{2+}/\text{Fe}^{3+}$ ratio of the start and end slag for A is 10. For the other experiment, the same ratio is assumed.

Table I. Composition (Weight Percent) and the NBC/NFC Ratio of the Industrial Nonferrous Slag As Received

Al_2O_3	CaO	Total Fe	MgO	SiO_2	ZnO	NBC/NFC
6.35	18.15	26.00	1.35	25.60	5.41	1.48

Table II. Composition and the NBC/NFC Ratio of the Start and End Slag for Experiment A

Weight Percent	Al_2O_3	CaO	Total Fe	MgO	SiO_2	ZnO	NBC/NFC
Start slag for A	6.95	18.80	26.10	1.30	26.20	5.48	1.52
End slag for A	7.45	18.75	25.55	1.35	26.00	5.35	1.51

Table III. Composition and the NBC/NFC Ratio of the Start and End Slag for Experiment B

Weight Percent	Al_2O_3	CaO	Total Fe	MgO	SiO_2	ZnO	NBC/NFC
Start slag for B	6.70	19.20	25.90	1.25	26.55	5.60	1.49
End slag for B	6.75	19.05	26.00	1.30	26.05	5.48	1.53

D. Thermodynamic Calculations

Thermodynamic calculations are performed with FactSage using the FACT53 and FACToxide databases.^[14] Only the main components SiO_2 , CaO, FeO_x , ZnO, Al_2O_3 , and MgO are considered. During the experiment no metallic lead phase is added. Furthermore a N_2 -gas is blown over the slag bath. Because of the large amount of slag bath (3 kg), it is assumed that the slag is not reduced by the gas. Analysis of the slag bath also show that the $\text{Fe}^{2+}/\text{Fe}^{3+}$ -ratio of the slag bath does not change during the experiment. Therefore, for the thermodynamic modeling, the slag is assumed not to be in contact with a second phase, like a gas or a metal, which results in a constant amount of oxygen (thus a $\text{Fe}^{2+}/\text{Fe}^{3+}$ -ratio) in the system as a function of temperature.

III. RESULTS

A. Microstructures

Microstructure types A and B are shown in Figure 4. They are taken from freeze layers A and B, but both microstructures are also observed at different parts within a same freeze layer.^[1] The phases present are indicated in Figure 5, and their chemical formulas are shown in Table IV.

In both microstructures, four zones can be distinguished. Zone 1 starts at the probe surface and consists of an amorphous matrix with small wüstite (rounded light gray) and spinel (faceted light gray) crystals. In zone 2, equiaxial crystals are observed in an amorphous matrix. They consist of wüstite, melilite (dark gray), spinel, and olivine (long thin gray) phases. In zone 3, columnar crystals dominate the microstructure. In microstructure type A (Figure 4(a)), these crystals consist of melilite, which forms large and broad crystals with a limited amount of matrix in between. The fraction of melilite increases with distance to the probe,

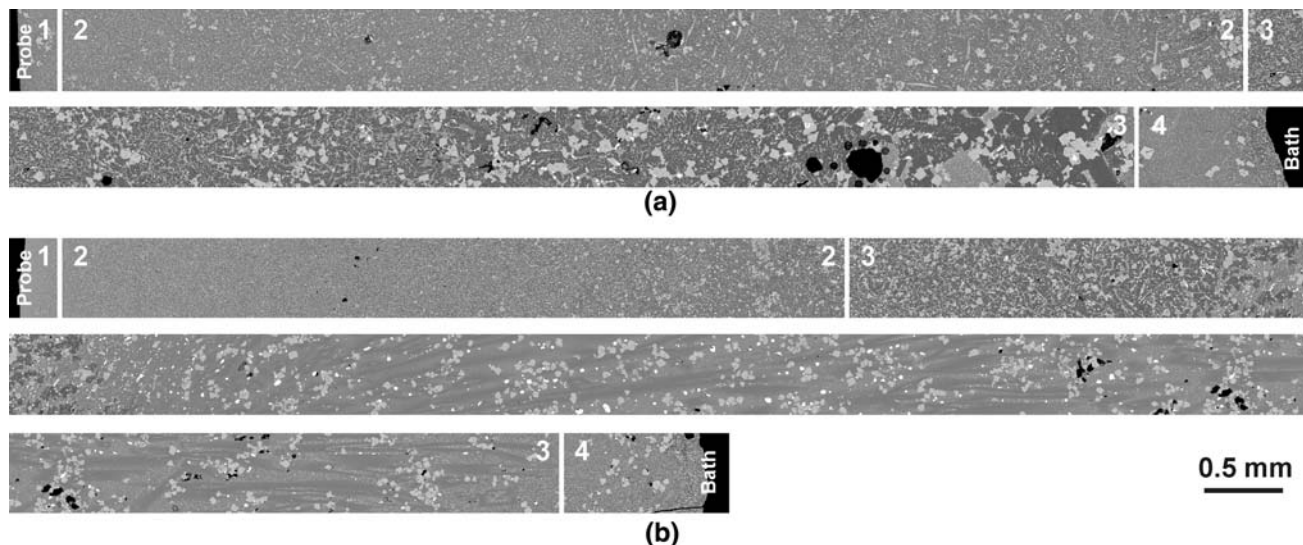


Fig. 4—Two types of microstructures. In both, four zones can be distinguished: (1) amorphous matrix with small crystals, (2) equiaxial crystals, (3) columnar crystals, and (4) amorphous matrix with small crystals similar to zone 1. The phases present are indicated in Fig. 5.

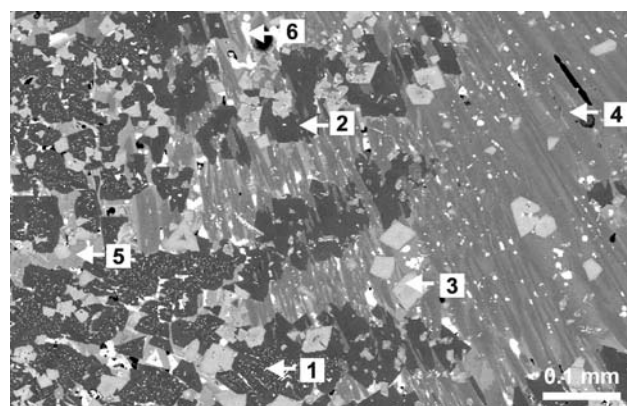


Fig. 5—Phases that can be observed in the microstructures shown in Fig. 4. (1) Dark gray melilite crystals with small light gray wüstite crystals, (2) dark gray melilite crystals, (3) light gray faceted spinel crystals, (4) long thin gray olivine crystals, (5) amorphous matrix, and (6) white matte droplets.

Table IV. Chemical Formulas of the Oxide Phases Observed in the Microstructures

Oxide Phase	Chemical Formula	NBC/NFC
Wüstite	Fe_{1-x}O	—
Melilite	$(\text{Ca})_2(\text{Fe, Zn, Mg, Al})_1(\text{Si, Al})_2\text{O}_7$	1.5
Spinel	$(\text{Mg, Zn, Fe, Ca})_1(\text{Fe, Al})_2\text{O}_4$	—
Olivine	$(\text{Fe, Ca, Zn, Mg})_2\text{Si}_1\text{O}_4$	2

while the fraction of matrix decreases and the fractions of spinel and of wüstite remain the same. In the second microstructure type (Figure 4(b)), the columnar crystals close to the probe consist of melilite, but further from the probe, they consist of olivine. These olivine columnar crystals are thin and long with a large amount of matrix in between. The fraction of olivine crystals

decreases with distance to the probe, while the fraction of matrix increases and the fractions of wüstite and of spinel crystals remain the same. Zone 4 is located at the liquid bath side and consists of an amorphous matrix with small wüstite and spinel crystals. In microstructure type B also, some small melilite crystals are observed.

During the experiment, the phase indicated as amorphous matrix in the four zones was a liquid or a glass. The liquid transformed to a glass during cooling and the original interface between liquid and glass cannot be distinguished afterward. Therefore, the term (amorphous) matrix is further used to indicate both the liquid and the glass phase.

B. Element Distribution

The distribution of SiO_2 , CaO , FeO_x , ZnO , Al_2O_3 , MgO , K_2O , and MnO in the melilite, olivine, and spinel crystals and in the matrix is determined as a function of distance to the probe. The wüstite, matte, and some spinel crystals, being too small, could not be analyzed. These small crystals cause some scatter in the matrix composition. In the element distribution graphs, the four zones observed in the microstructures are indicated. For microstructure B, a distinction is made between zone 3 with melilite columnar crystals (= 3M) and zone 3 with olivine columnar crystals (= 3O).

The distribution of CaO is shown in Figures 6(a) and (b). The spinel crystals contain no CaO , so these data points are not shown. In zones 1 and 2, the CaO concentration in the matrix increases with distance to the probe. When melilite, which has a higher CaO concentration than the slag bath, is present in zone 3 (3M), the matrix depletes in CaO . For microstructure A, the CaO amount in the matrix of zone 4 increases with distance to the probe and reattains the bath concentration at the end of the zone. In zone 3O of microstructure B, the CaO concentration in olivine is higher than in the

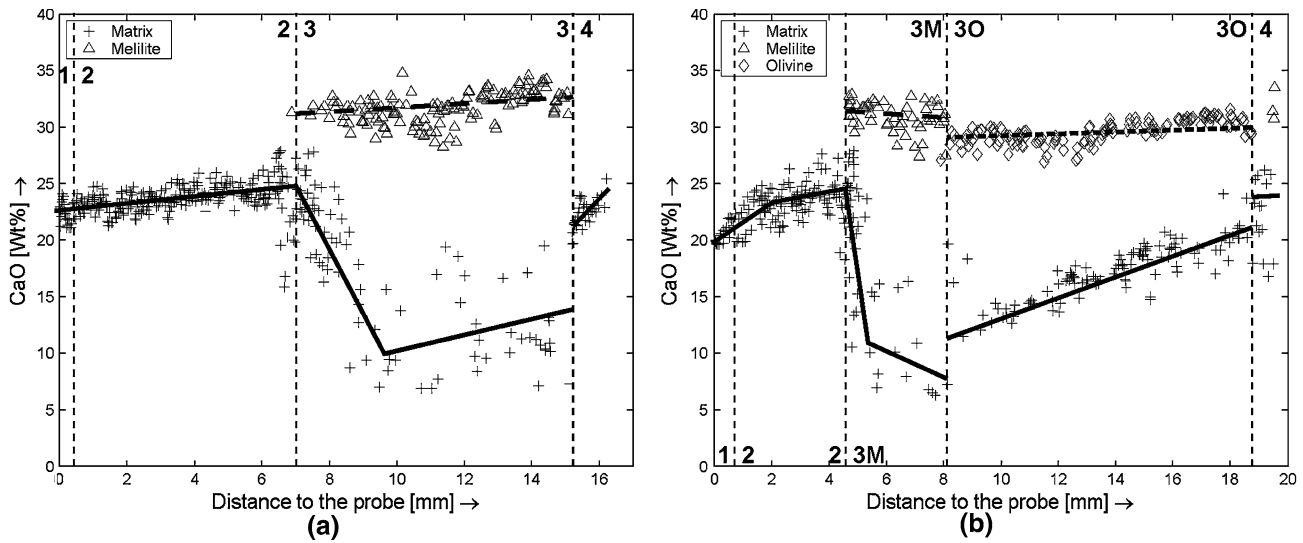


Fig. 6—CaO distribution (a) in freeze layer A with melilite columnar crystals and (b) in freeze layer B with melilite and olivine columnar crystals. The full, the dashed and the dotted lines show the interpolation of the matrix concentration, the melilite concentration, and the olivine concentration respectively.

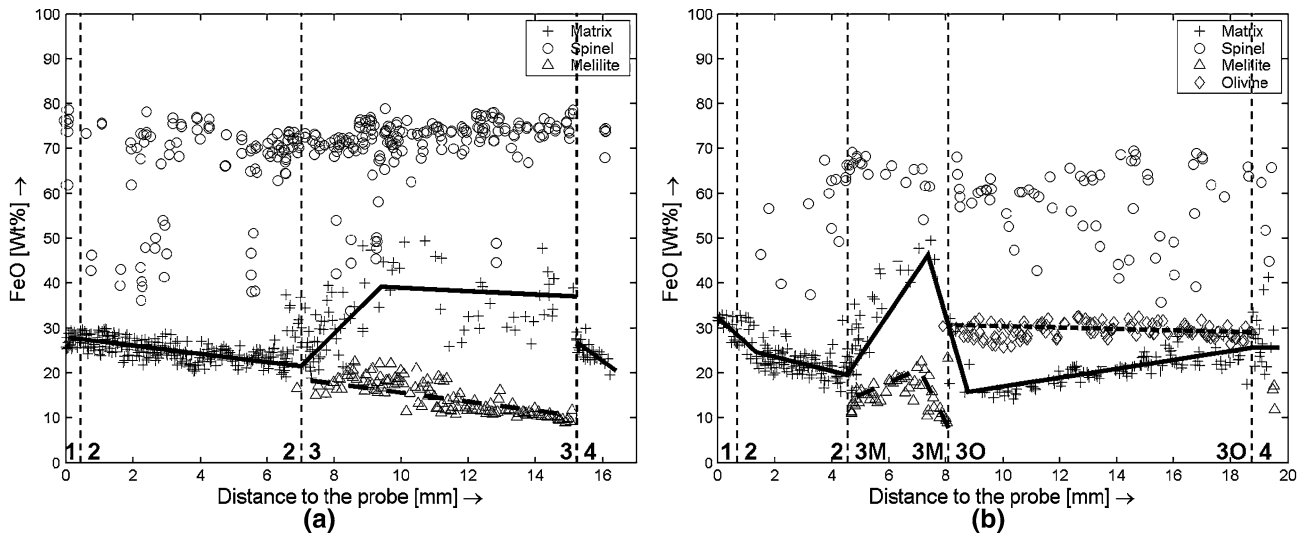


Fig. 7—FeO distribution (a) in freeze layer A with melilite columnar crystals and (b) in freeze layer B with melilite and olivine columnar crystals. All iron is shown as FeO. The full, the dashed and the dotted lines show the interpolation of the matrix concentration, the melilite concentration, and the olivine concentration respectively.

matrix and remains constant. In the matrix, the concentration increases to reach the bath concentration at the end of zone 3 and remains constant in zone 4.

The FeO concentration in the matrix of zones 1 and 2 decreases with the distance to the probe, as shown in Figure 7. When melilite crystals, which contain less FeO than the slag bath, are present, the matrix enriches in FeO. For microstructure B, the FeO concentration in the melilite crystals strongly decreases at the end of zone 3M. In zone 4 of microstructure A, the FeO concentration in the matrix decreases with distance to the probe to reattain the bath concentration at the end of the zone. In zones 3O and 4 of microstructure B, FeO distributes similarly to CaO. In the spinel crystals of all zones, the

FeO concentration remains constant and is higher than in the slag bath.

In zones 1 and 2, the K_2O concentration slightly increases with distance to the probe, as shown in Figure 8. When melilite, which has a lower K_2O concentration than the matrix, is present, the matrix enriches in K_2O . In zone 4 of microstructure A, the K_2O concentration in the matrix decreases with distance to the probe. For microstructure B, the matrix strongly enriches in K_2O , when olivine crystals are present. Here, the K_2O concentration decreases with distance to the probe. In between two parallel olivine crystals, the K_2O has a maximum concentration at the crystal-matrix interface and a minimum concentration in the middle

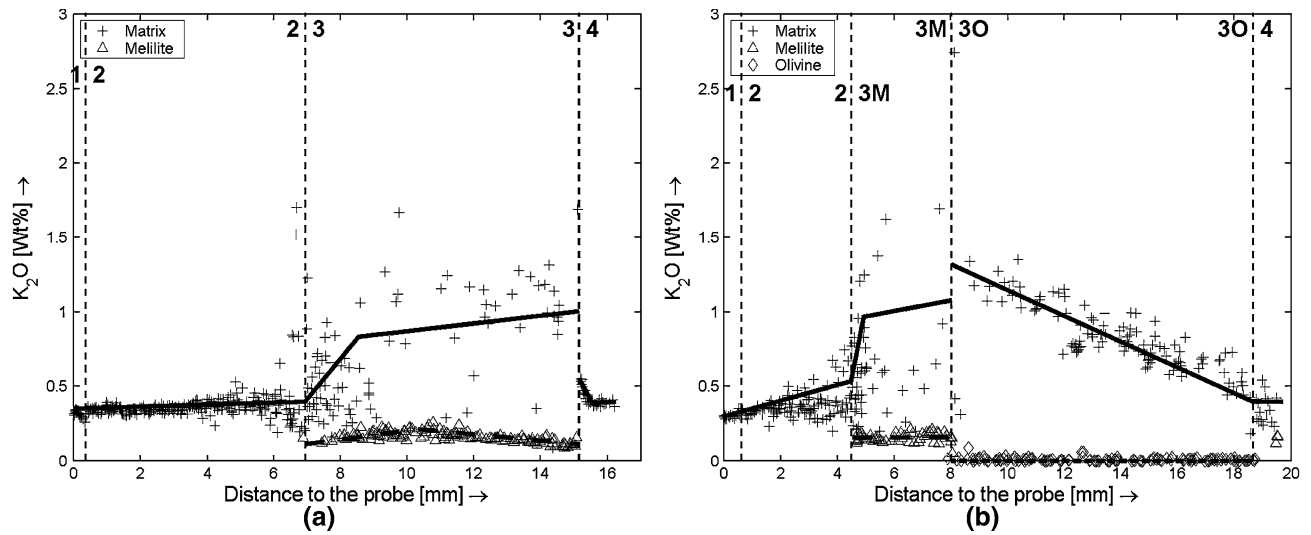


Fig. 8—The K_2O distribution (a) in freeze layer A with melilite columnar crystals and (b) in freeze layer B with melilite and olivine columnar crystals. The full, the dashed and the dotted lines show the interpolation of the matrix concentration, the melilite concentration, and the olivine concentration respectively.

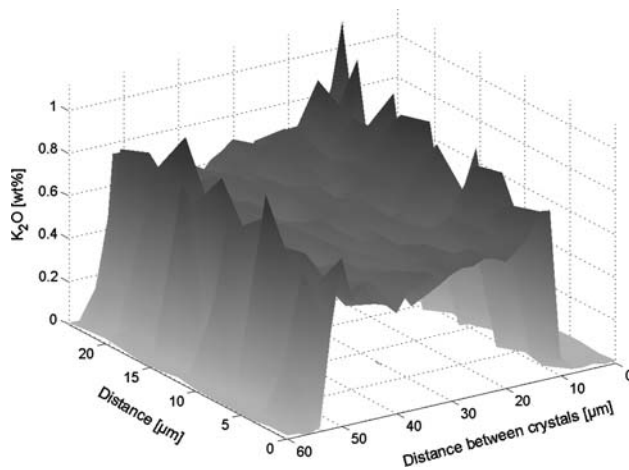


Fig. 9— K_2O distribution in the matrix between two parallel olivine columnar crystals in zone 3O. A small part of the crystals is shown at the left (approximately, 55 to 60 μm) and at the right side (approximately, 0 to 10 μm) of the figure. The distance between the columnar crystals is 45 μm .

between the crystals, as shown in Figure 9. In zone 4, the matrix has a constant K_2O concentration. Both the olivine and spinel crystals do not contain K_2O . The data points are not shown for the spinel phase.

For the other components, a similar behavior as for CaO, FeO, or K_2O is observed. In zones 1 and 2, Al_2O_3 and ZnO behave similarly to FeO, and SiO_2 behaves similarly to CaO and K_2O . MgO and MnO have a constant concentration in the matrix and, here, the concentration in the spinel crystals equals the bath composition. In zones 3 and 4 of microstructure A, ZnO, MgO, and SiO_2 behave similarly to CaO, while MnO behaves similarly to FeO and K_2O . The Al_2O_3 concentration in the matrix decreases, and in the melilite crystals, it is equal to the bath concentration. Zone 4 of microstructure A shows a slightly increasing Al_2O_3

concentration in the matrix with distance to the probe. In zone 3M of microstructure B, the components behave similarly as in zone 3 of microstructure A, but here, at the end of zone 3M, a strong change in melilite composition is observed for some components. The SiO_2 , ZnO, and MgO concentrations strongly increase, while the Al_2O_3 concentration strongly decreases as for FeO. In zones 3O and 4, Al_2O_3 and ZnO behave similarly to K_2O while MgO and MnO behave similarly to CaO and FeO. The SiO_2 concentration in the matrix equals its concentration in the olivine crystals, and the matrix composition is constant in zone 4.

IV. DISCUSSION

In Sections A through C, first, the element distribution is interpreted and the mass transport of the elements is discussed for the different zones in the freeze layers. Then, the influence of mass transport on crystal growth is considered. Finally, the implications of the mass transport on freeze lining application are discussed.

A. Mass Transport in the Freeze Lining

A distinction is made between short-range and long-range mass transport. Short-range mass transport is the local exchange of components between the liquid slag and the crystals without changing the global composition of the freeze layer. Long-range mass transport is the exchange of components parallel to the direction of the heat flux resulting in a change in the global composition of the freeze layer.

In zones 1 and 2 of both microstructure types, the matrix depletes, for example, in FeO; thus, FeO is transported away from the matrix. FeO can be transported from the freeze layer to the liquid bath, so the

complete freeze layer depletes in FeO. The concentration can also change due to the formation of FeO-rich crystals. In these zones, the solidification rate is high and the slag is cooled to a low temperature.^[1] Furthermore, the crystals in these zones are rich in FeO (mostly wüstite and spinel phase). Therefore, the FeO depletion of the matrix is mainly due to short-range mass transport. This depletion is stronger with increasing distance to the probe, because the crystalline fraction increases. Al₂O₃ and ZnO behave similarly to FeO, because the crystals are rich in these components; while CaO, K₂O, and SiO₂ behave oppositely to FeO, because the crystals are poor in these components. The MgO and MnO concentrations in the matrix remain constant, because their concentration in the crystals equals their concentration in the bath.

In zone 3, the solidification rate is lower and the slag is at a higher temperature than in zones 1 and 2. As a result, the impact of mass transport is larger. In microstructure A, melilite contains, for example, less FeO than the bath, so FeO enriches in the matrix, as is schematically shown by the full line in the graph of Figure 10(a). The fraction of melilite crystals increases, while the FeO concentration in melilite decreases with distance to the probe. Also, the fraction of matrix

decreases with distance to the probe, while the FeO concentration in the matrix remains constant. Furthermore, the fraction of spinel and wüstite crystals remains constant and also the FeO fraction in the spinel crystals remains constant. Because the freeze layer composition in the beginning of zone 3 is close to the bath composition, the freeze layer at the bath side seems to contain less FeO than the bath.

Together with the concentration gradient in zone 4, these observations imply long-range mass transport of FeO from the freeze layer to the bath, as indicated by the arrows in Figure 10(a). K₂O and MnO show the same behavior and CaO, SiO₂, ZnO, and MgO show the opposite behavior. Al₂O₃ behaves differently, because the matrix depletes in Al₂O₃ while its concentration in the melilite is not higher than in the slag bath. Here, the spinel crystals contain remarkably more Al₂O₃ than the slag bath. For all components, the total exchange with the bath, however, is limited, because the start and end slag bath compositions are equal, as shown in Table II.

In zone 3M of microstructure type B, the mass transport of the components is similar to zone 3 of microstructure type A. When olivine is present, a different mass transport is observed. K₂O, for example, is not present in the olivine phase, so the matrix strongly

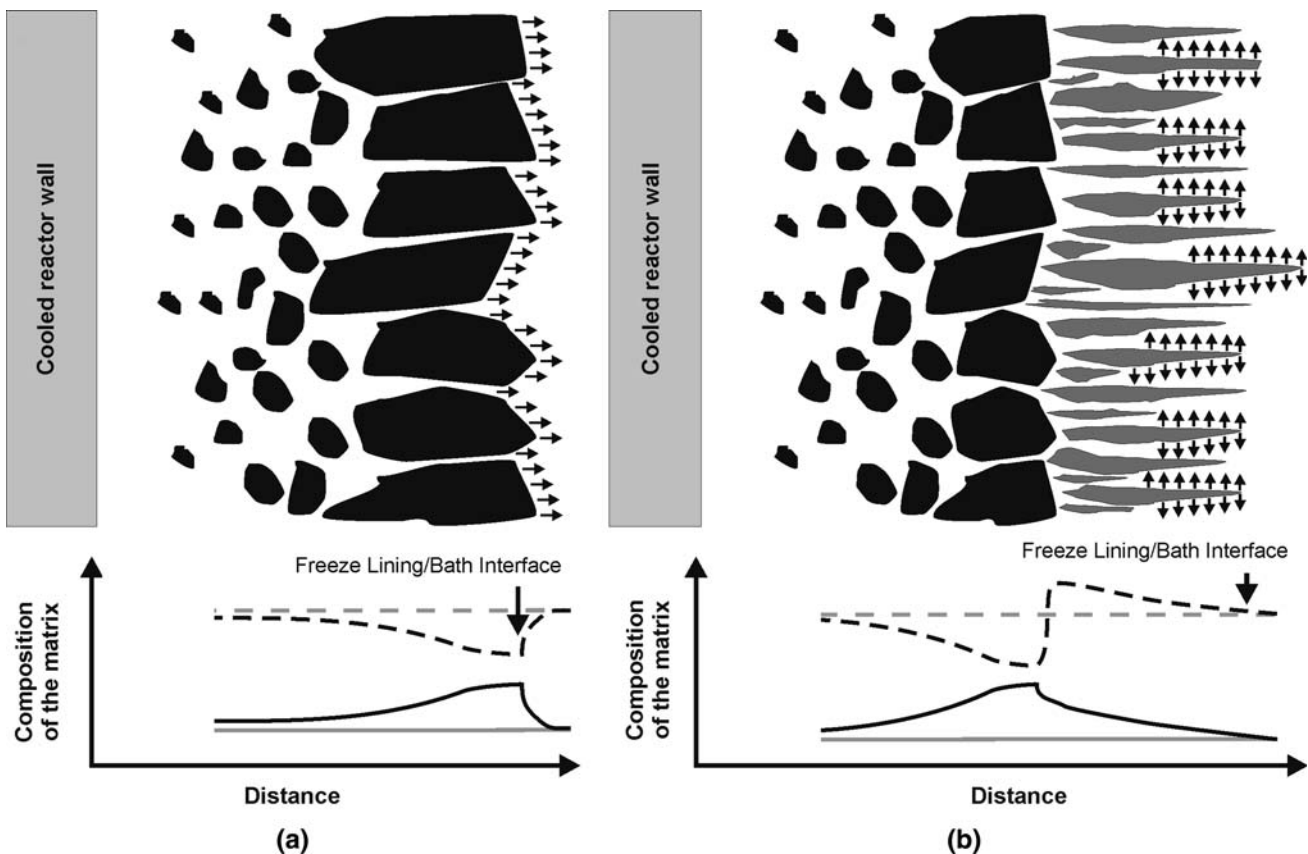


Fig. 10—Schematic representation of the mass transport in zone 3 (a) for the microstructure with melilite (black) columnar crystals and (b) for the microstructure with melilite and olivine (gray) columnar crystals. The arrows indicate the mass transport from the columnar crystals to the matrix (white). Typical composition profiles of the matrix are shown in the graphs (black) and are compared with the bath composition (gray). In (a), the full line is of components that enrich in the matrix when melilite crystals form, and the dashed line is for components that deplete in the matrix. In (b), the full line is for components that enrich in the matrix when melilite crystals form, and the dashed line is for components that deplete in the matrix; however, in the presence of olivine crystals, both lines are for components that enrich in the matrix.

enriches in K_2O (similar to the full line in Figure 10(b)). This enrichment decreases with distance to the probe. In zone 4, the composition equals the bath composition and no gradient is observed. Olivine forms thin long crystals with a large amount of matrix in between, and the crystalline fraction decreases with distance to the probe. The matrix between two parallel olivine crystals shows gradients (Figure 9). Here, the mass transport is mostly short range between olivine and the local matrix, which consists of liquid slag entrapped between the olivine crystals. This mass transport is shown by the arrows in Figure 10(b). Long-range mass transport between the freeze layer and bath is limited. Here, also, no change of bath composition is observed, as shown in Table III. Al_2O_3 behaves similarly to K_2O . CaO , FeO , MgO , SiO_2 , and MnO are transported in the opposite direction of K_2O from the local matrix to the crystals.

B. Growth of the Crystalline Phases

In zones 1 and 2, the impact of mass transport is limited, because, here, the freeze layer growth is heat transfer controlled and a large part of the slag solidifies as a glass phase. Therefore, only the crystal growth in zone 3 will be discussed further. When melilite crystals grow, a major part of the melilite inhibiting components (which have a lower concentration in melilite than in the bath) pile up at the melilite crystal-matrix interface. The melilite favoring components (which have a higher concentration in melilite than in the bath), on the contrary, run short in the matrix close the crystals. The amount of matrix between the melilite crystals, however, is limited; thus, most of the components have to be exchanged with the liquid slag bath. Thus, the transport of both favoring and inhibiting components between the bath and the freeze layer inhibits the growth of the melilite crystals and results in an undercooling and a change in composition of the

liquid slag at the melilite-bath interface.^[15] The olivine inhibiting components, on the contrary, mostly can be transported to the matrix between the crystals, as the arrows in Figure 10(b) show. As a result, both the change in composition and the undercooling at the olivine crystal-liquid bath interface are limited.

The reason why in one case only melilite columnar crystals form and in another case also olivine columnar crystals form is not clear. The mass transport of the components can provide an explanation. In both cases, the first columnar crystals that form are of melilite phase. Although this is not the primary phase, as shown in the calculated solidification path in Figure 11, melilite formation is not unreasonable, because its composition is close to the bath composition (same NBC/NFC as slag bath, Tables I and IV) and thus its formation and growth require limited mass transport. As stated previously, the local composition at the crystal-liquid bath interface can change or undercool. This change in composition might result in the olivine phase becoming more stable than the melilite phase. The results show that compared to the bath composition, the FeO concentration in the matrix strongly increases in the presence of melilite, the SiO_2 slightly increases, and the CaO concentration strongly decreases. According to thermodynamic calculations (Figure 12), a combination of these changes results in olivine forming at a higher temperature than melilite. Also, the liquid at the freeze layer-bath interface undercools. If melilite nucleation is strongly suppressed, olivine becomes the second phase to form (Figure 13). In the element distributions, a change in melilite composition is observed at the end of zone 3M of microstructure type B. The SiO_2 concentration strongly increases, while the Al_2O_3 and FeO concentrations strongly decrease. This might imply that the local concentration of melilite promoting components was beneath some critical value or that the liquid

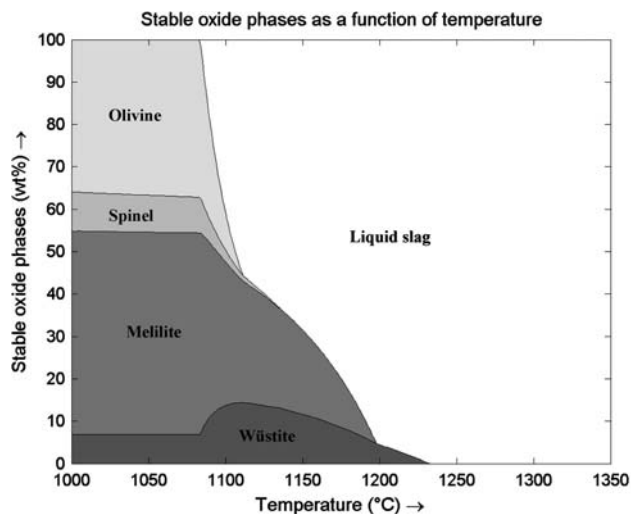


Fig. 11—Equilibrium solidification path of the industrial nonferrous slag. The path shows the fraction of oxide phases as a function of temperature in case the slag is infinitely slow cooled and the diffusion in all phases is infinitely fast. For the calculations, the slag composition in Table I is used with a Fe^{2+}/Fe^{3+} ratio of 10.

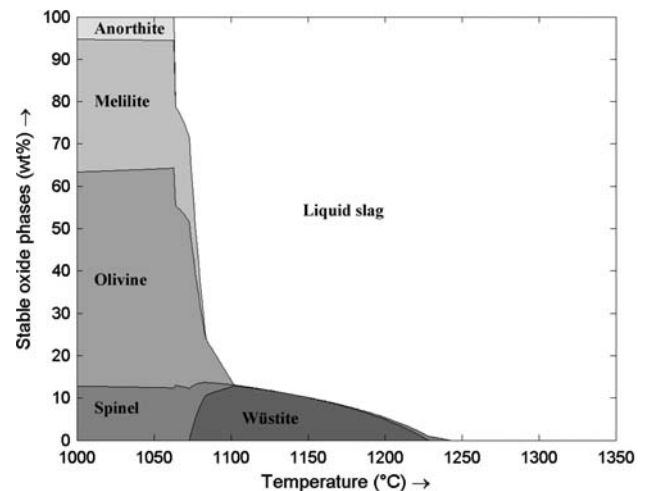


Fig. 12—Equilibrium solidification path of the slag at the melilite crystals-slag bath interface. The concentrations of CaO , Fe , and SiO_2 are changed according to the change in the matrix composition between the melilite crystals (6 wt pct ZnO , 29.2 wt pct SiO_2 , 7 wt pct Al_2O_3 , 1.5 wt pct MgO , 14 wt pct CaO , 32.6 wt pct Fe , and a Fe^{2+}/Fe^{3+} ratio of 10).

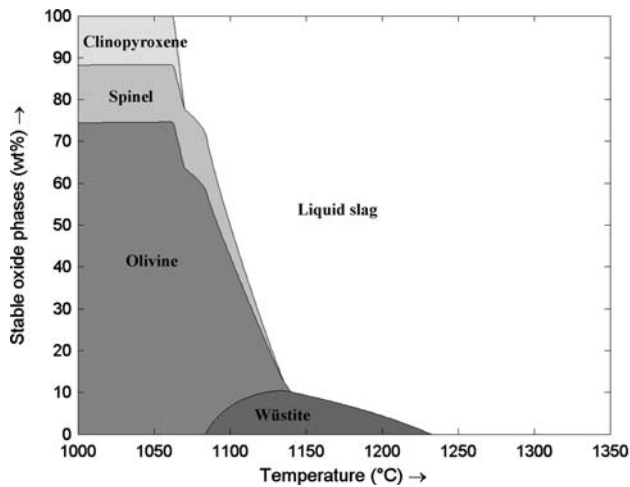


Fig. 13—Equilibrium solidification path of the industrial nonferrous slag when the melilite formation is suppressed. Here, similarly to the normal equilibrium solidification path (Fig. 11), the slag composition in Table I with a $\text{Fe}^{2+}/\text{Fe}^{3+}$ ratio of 10 is used for the calculations. The difference is that melilite is not selected as a possible phase to form.

was locally at a critical temperature so olivine nucleated. In microstructure type A, this critical concentration or temperature was not reached and melilite could grow normally. When olivine crystals form, they dominate the microstructure. Olivine has a simpler crystal structure than melilite,^[16] so molecules can more easily attach to its crystals.

What is remarkable is that not only the mass transport of the main components is important but that also the mass transport of minor components can have a strong effect. For example, the K_2O concentration at the olivine crystal-bath interface can rise from approximately 0.3 to 1.5 wt pct, because K_2O is not present in olivine. For olivine crystals to grow, K_2O has to be transported away from the interface to the bulk bath. Thus, the mass transport of K_2O inhibits the growth of the olivine crystals. Similar behavior is observed for other minor components.

C. Implications for Freeze Lining Application

As the solidification rate of the slag decreases with distance to the probe, correspondingly, the influence of mass transport on freeze lining growth increases. Furthermore, the mass transport occurs in a different way for different dominating phases in the microstructure. This is determined by the crystal morphology of the phase and the difference in composition between the phase and the bath.

Dependent on the dominating phase in the microstructure, the freeze layer shows a different structure and different properties. Melilite forms a closed structure with a small amount of matrix in between the crystals. Therefore, it might be more difficult for liquid slag to penetrate in the freeze layer and reach the refractory material. Olivine on the contrary forms an open structure with a large amount of matrix in between the crystals. Therefore, liquid slag may more easily

penetrate in the freeze layer and come in contact with refractory. If the temperature at the reactor wall is above the glass temperature, this risk increases.

In previous research, it was considered that the temperature at the freeze layer-bath interface is lower than the liquidus temperature during the formation of the freeze layer, because the freeze layer does not consist of primary phase.^[1] The results here show that the freeze layer does not even show the tendency to enrich in primary phase for both microstructure types, because in both cases, the freeze layer does not enrich in FeO , although it is the main component of the primary phase wüstite (Table IV).

V. CONCLUSIONS

In order to explore the phenomena that appear in an industrial freeze lining, the element distribution in two microstructure types, one with melilite columnar crystals and the other with melilite and olivine columnar crystals, is investigated. The element distribution, the phase fraction, and the crystal morphology give important information on the mass transport in the freeze layers.

In the zones with amorphous matrix and small crystals, only short-range mass transport is important and the growth of the freeze layer is dominated by heat transport. In the zone with columnar crystals, long-range mass transport influences the growth of the freeze layer. Here, different growth mechanisms are observed for the melilite and the olivine columnar crystals, which have a different crystal morphology and structure. Melilite forms a close network of large broad crystals with a small amount of matrix in between the crystals. As a result, the freeze layer has to exchange components with the liquid slag bath to grow. Olivine forms an open network of long thin crystals with a large amount of matrix in between the crystals. Here, the freeze layer does not have to exchange components with the liquid slag bath, but it can exchange components with the local matrix in between the crystals.

Furthermore, the mass transport of minor elements can have a significant influence on the growth of the crystalline phase, when they pile up at the crystal-liquid interface.

REFERENCES

1. M. Campforts, K. Verscheure, E. Boydens, T. Van Rompaey, B. Blanpain, and P. Wollants: *Metall. Mater. Trans. B*, 2007, vol. 38B, pp. 841–51.
2. L.R. Nelson, R. Sullivan, P. Jacobs, E. Munnik, P. Lewarne, E. Roos, M.J.N. Uys, B. Salt, M. de Vries, K. McKenna, N. Voermann, and B.O. Wasmund: *J. South Afr. Inst. Min. Metall.*, 2004, vol. 104 (9), pp. 551–61.
3. D.G.C. Robertson and S. Kang: *Fluid Flow Phenomena in Metals Processing*, San Diego, CA, 1999, TMS, Warrendale, PA, 1999, pp. 157–68.
4. K. Verscheure, M. Van Camp, B. Blanpain, P. Wollants, P. Hayes, and E. Jak: *Metall. Mater. Trans. B*, 2007, vol. 38B, pp. 13–20.
5. K. Verscheure, M. Van Camp, B. Blanpain, P. Wollants, P. Hayes, and E. Jak: *Metall. Mater. Trans. B*, 2007, vol. 38B, pp. 21–33.

6. J.H. Zietsman and P.C. Pistorius: *Miner. Eng.*, 2006, vol. 19, pp. 262–79.
7. P.C. Pistorius: *Proc. VII Int. Conf. on Molten Slags, Fluxes and Salts*, Cape Town, South Africa, 2004, SAIMM, Johannesburg, South Africa, 2004, pp. 237–42.
8. P.C. Pistorius: *J. South Afr. Inst. Min. Metall.*, 2003, vol. 103 (8), pp. 509–14.
9. K.A. Rye, T. Eidet, and K. Tørklep: *Light Metals 1999*, San Diego, CA, 1999, TMS, Warrendale, PA, 1999, 347–52.
10. C.C. Wei, J.J.J. Chen, B.J. Welch, and V.R. Voller: *Light Metals 1997*, Orlando, FL, 1997, TMS, Warrendale, PA, 1997, pp. 309–16.
11. A. Solheim and L.I.R. Støen: *Light Metals 1997*, Orlando, FL, 1997, TMS, Warrendale, PA, 1997, pp. 325–32.
12. J. Thonstad and S. Rolseth: *Light Metals 1983*, New York, NY, 1983, TMS-AIME, Warrendale, PA, 1983, pp. 415–23.
13. K. Verscheure, M. Campforts, F. Verhaeghe, E. Boydens, M. Van Camp, B. Blanpain, and P. Wollants: *Metall. Mater. Trans. B*, 2006, vol. 37B, pp. 929–40.
14. C.W. Bale, P. Chartrand, S.A. Degterov, G. Eriksson, K. Hack, R. Ben Mahfoud, J. Melançon, A.D. Pelton, and S. Petersen: *Calphad*, 2002, vol. 26 (2), pp. 189–228, www.factsage.com.
15. W. Kurz and D.J. Fisher: *Fundamentals of Solidification*, 3rd ed., Trans Tech Publishers, Aedermannsdorf, Switzerland, 1989.
16. W.A. Deer, R.A. Howie, and J. Zussman: *An Introduction to the Rock-Forming Minerals*, 2nd ed., Longman Scientific & Technical, London, 1992, pp. 3–15 and 108–13.